Amyloid and Tau PET Demonstrate Region-Specific Associations in Normal Older People

Samuel N. Lockhart[a,*], **Michael Schöll**[a,b], **Suzanne L. Baker**[a,c], **Nagehan Ayakta**[d], **Kaitlin N. Swinnerton**[a,c], **Rachel K. Bell**[a], **Taylor J. Mellinger**[a,c], **Vyoma D. Shah**[a,c], **James P. O'Neil**[c], **Mustafa Janabi**[c], and **William J. Jagust**[a,c]

[a]Helen Wills Neuroscience Institute, University of California Berkeley, Berkeley, California, 94720, USA

[b]MedTech West and the Department of Clinical Neuroscience and Rehabilitation, University of Gothenburg, 405 30 Gothenburg, Sweden

[c]Lawrence Berkeley National Laboratory, Berkeley, California, 94720, USA

[d]Department of Neurology, Memory and Aging Center, University of California San Francisco, San Francisco, California, 94158, USA

Abstract

β-amyloid (Aβ) and tau pathology become increasingly prevalent with age, however, the spatial relationship between the two pathologies remains unknown. We examined local (same region) and non-local (different region) associations between these 2 aggregated proteins in 46 normal older adults using $[^{18}F]$AV-1451 (for tau) and $[^{11}C]$PiB (for Aβ) positron emission tomography (PET) and 1.5T magnetic resonance imaging (MRI) images. While local voxelwise analyses showed associations between PiB and AV-1451 tracer largely in the temporal lobes, k-means clustering revealed that some of these associations were driven by regions with low tracer retention. We followed this up with a whole-brain region-by-region (local and non-local) partial correlational analysis. We calculated each participant's mean AV-1451 and PiB uptake values within 87 regions of interest (ROI). Pairwise ROI analysis demonstrated many positive PiB—AV-1451 associations. Importantly, strong positive partial correlations (controlling for age, sex, and global gray matter fraction, $p < .01$) were identified between PiB in multiple regions of association cortex and AV-1451 in temporal cortical ROIs. There were also less frequent and weaker positive associations of regional PiB with frontoparietal AV-1451 uptake. Particularly in temporal lobe ROIs, AV-1451 uptake was strongly predicted by PiB across multiple ROI locations. These data indicate that Aβ and tau pathology show significant local and non-local regional associations among cognitively normal elderly, with increased PiB uptake throughout the cortex correlating with increased temporal lobe AV-1451 uptake. The spatial relationship between Aβ and tau accumulation does

*Corresponding author: Samuel N. Lockhart; 132 Barker Hall, MC#3190, University of California, Berkeley, California, 94720, USA.

not appear to be specific to Aβ location, suggesting a regional vulnerability of temporal brain regions to tau accumulation regardless of where Aβ accumulates.

Keywords

Aging; tau; amyloid; PET; Alzheimer's Disease; polypathology

1. Introduction

In addition to their association with Alzheimer's disease (AD), β-amyloid (Aβ) and tau pathologies become increasingly prevalent in the human brain with advanced age (Davis et al., 1999; Bennett et al., 2006). Nevertheless, the spatial relationship between the two pathologies remains poorly understood. *In vivo* amyloid imaging has been implemented for over a decade (Klunk et al., 2004); the recent development of tau PET ligands which bind to paired helical filament (PHF) forms of tau now enable the examination of regional pathological associations between these two aggregated proteins in cognitively normal elderly (Chien et al., 2013; Johnson et al., 2015; Ossenkoppele et al., 2016; Schöll et al., 2016; Schwarz et al., 2016). These and other polypathology studies appear to indicate that globally increasing Aβ burden precedes and is associated with greater accumulation of tau, particularly in the neocortex. However, the associations of regional and global amounts of Aβ with the topography of tau deposition remain unknown.

These relationships are important, having bearing on whether and how the accumulation of one protein might influence the accumulation of the other. For example, different conclusions about the spread of disease pathology throughout the brain may be drawn if Aβ and tau are locally correlated, as opposed to the situation in which Aβ may affect tau deposition in remote (non-local) areas. The regional specificity in Aβ-tau relations may inform our understanding of the biological mechanisms of disease pathology in both aging and disease. These relationships have important implications for monitoring the progression of AD, designing clinical trials of AD therapeutics, and diagnosing the earliest stages of AD as distinct from normal cognitive aging.

In this study, we used the well-known PET amyloid imaging agent [^{11}C]Pittsburgh Compound B (PiB) along with the more recently developed tau PET tracer [^{18}F]AV-1451 to map and compare the regional depositions of Aβ and tau. We hypothesized, based on previous *in vivo* and *post mortem* evidence, that the relationships between PiB and AV-1451 uptake patterns would be such that diffuse patterns of Aβ deposition were associated with more regional, focal effects on tau pathology. Specifically, we hypothesized that the spatial distribution of strong associations would be selectively dependent on tau localization, suggesting Aβ effects on regions that are particularly vulnerable to the aggregation of tau.

We examined cross-sectional inter-regional association patterns between Aβ and tau. We quantified local (same region) and non-local (different region) associations between PiB (Aβ) and AV-1451 (tau) PET in normal aging. Specifically, we used Biological Parametric Mapping (BPM; Casanova et al., 2007; Yang et al., 2011) robust multiple regressions to assess local associations, and we used region of interest (ROI)-based partial correlations to

assess both local and non-local associations. These approaches, similar to examinations of "local" and "distributed" associations described in previous literature (Sepulcre et al., 2013; Sepulcre et al., 2016) had the aim of characterizing how the spatial locations of these two pathological proteins are related.

2. Material and methods

2.1. Participants

We recruited 46 cognitively normal older adults (OA; 78.8 +/− 5.1 y age, 16.2 +/− 1.8 y education, 31 female, Mini-Mental State Examination [MMSE] score 28.6 +/− 1.3) from the ongoing longitudinal Berkeley Aging Cohort Study (Mormino et al., 2009). All participants underwent structural MRI, and [^{11}C]PiB and [^{18}F]AV-1451 PET imaging (see section 2.2). Eligibility requirements included the following: no imaging contraindications, community-dwelling, study entry MMSE score ≥ 25 normal performance on cognitive tests (< 1.5 SD of normative values on the California Verbal Learning Test [Delis et al., 2000] or Wechsler Memory Scale Delayed Recall [Wechsler, 1997]), absence of neurological or psychiatric illness, and lack of major medical illnesses and medications affecting cognition. The Institutional Review Boards of all participating institutions approved the study and informed consent was obtained from all participants.

2.2. Image Acquisition

[^{11}C]PiB was synthesized at the Lawrence Berkeley National Laboratory (LBNL) Biomedical Isotope Facility, using a previously described protocol (Mathis et al., 2003). PiB PET imaging was performed in 3D acquisition mode using either an ECAT EXACT HR scanner ($n = 6$) or a BIOGRAPH PET/CT Truepoint 6 scanner ($n = 40$, both Siemens Medical Systems, Erlangen, Germany). PiB distribution volume ratio (DVR) values are not significantly different between scanners used (Elman et al., 2014). Immediately after intravenous injection (~15 mCi) of PiB, 90 min of dynamic acquisition frames were obtained (4×15, 8×30, 9×60, 2×180, 10×300, and 2×600 s). For each PiB scan, a PET transmission scan or computed tomography (CT) scan was obtained for attenuation correction, with images reconstructed using an ordered subset expectation maximization algorithm with weighted attenuation, scatter correction, and smoothed with a 4 mm Gaussian kernel.

[^{18}F]AV-1451 PET imaging was performed within a mean of 75.3 (+/− 110) days of PiB PET. AV-1451 was synthesized at LBNL using a GE TracerLab FXN-Pro synthesis module based on a protocol supplied by Avid Radiopharmaceuticals. AV-1451 imaging was conducted on the BIOGRAPH PET/CT scanner; BIOGRAPH data are collected in list mode, with time frame data binned into 4x5 min frames during reconstruction to produce precisely 80–100 min AV-1451 data (for SUVR calculation, see section 2.3.2). Participants were injected with 10 mCi of tracer and participated in one of two acquisition schemes, using either full dynamic scans ($n = 23$; 0–100 min postinjection with 4×15 s, 8×30 s, 9×60 s, 2×3 min, and 16×5 min frames; and 120–150 min, 6×5 min frames), or 75–115 min scans ($n = 23$; 8×5 min frames). AV-1451 PET data were attenuation corrected with CT. Images were

reconstructed using an ordered subset expectation maximization algorithm with weighted attenuation, scatter correction, and smoothed with a 4 mm Gaussian kernel.

In addition, all participants underwent a high-resolution T1-weighted magnetization prepared rapid gradient echo (MPRAGE) scan (TR/TE = 2110/3.58 ms, FA = 15°, 1x1x1mm resolution) on a 1.5T Siemens Magnetom Avanto MRI scanner at LBNL.

2.3. PET Image Preprocessing

2.3.1. PiB—Images were realigned, and frames corresponding to the first 20 min of acquisition were averaged and coregistered to the participant's MRI. Native-space voxelwise DVR images were generated using Logan graphical analysis (35–90 min postinjection, cerebellar gray matter [GM] reference region; Logan et al., 1996; Price et al., 2005). We calculated global cortical PiB DVR values using native-space FreeSurfer-derived cortical GM masks, for each participant (Mormino et al., 2011); the range of global PiB DVR values was 0.932 to 1.81. A total of 23 subjects were classified as Aβ positive.

2.3.2. AV-1451—Data were realigned, and the mean of all frames was used to coregister AV-1451 data to each participant's MRI. We used different coregistration approaches for the separate acquisition schemes (0–150 min data used for participants with full dynamic scans, and 80–100 min data used for participants with 75–115 min scans); we visually confirmed that coregistration approach did not impact ROI segmentation. We created AV-1451 standardized uptake value (SUV) images based on mean tracer uptake over 80–100 min postinjection, then normalized SUV images to a cerebellar GM reference region (Chien et al., 2013; Schöll et al., 2016) to create native-space voxelwise SUV ratio (SUVR) images for each participant.

2.4. MRI Processing

We processed T1 MPRAGE scans using FreeSurfer version 5.1 (http://surfer.nmr.mgh.harvard.edu/) to delineate anatomical ROI masks for multiple brain regions on the native space MRI (coregistered to the PET scans; Mormino et al., 2009), and manually checked segmentations for accuracy. The cerebellar GM mask used as a reference region for PiB and AV-1451 PET was derived this way. MRI images were also segmented into brain tissue types using SPM8 (www.fil.ion.ucl.ac.uk/spm). We calculated a global GM fraction covariate (GM/intracranial volume), reflecting degree of whole-brain GM atrophy (one value per subject).

2.5. PET Data Template Space Normalization

We warped MRI scans for all OA to the FSL MNI152 2mm space template (www.fmrib.ox.ac.uk/fsl) using Advanced Normalization Tools (ANTS; http://stnava.github.io/ANTs/) with the use of a study-specific intermediate template (Schöll et al., 2016). After estimating transformations from each native space into MNI152 space, transformations were concatenated and applied to the MRI and coregistered AV-1451 and PiB PET images to generate MNI template space PET images.

2.6. BPM Analysis Preprocessing and Statistics

For BPM analysis, we focused on cortical AV-1451 binding patterns (putative off-target binding occurs in subcortical regions; Marquie et al., 2015; Schöll et al., 2016). BPM allows the use of voxelwise independent and dependent variable data (e.g., PiB and AV-1451 PET images), plus covariates of no interest, to analyze the statistical relations between variables, using robust regression methods (Casanova et al., 2007; Yang et al., 2011). We refer to these as local relationships, since BPM examines relationships between the 2 modalities within the same voxel(s). We employed a FreeSurfer segmentation on the MNI152 template structural MRI, and created a mask using all cortical GM brain regions, which was applied to the MNI template-space PET images produced above. To reduce contributions of CSF and noise in PET data to voxel-wise analysis, low signal-to-noise voxels at the GM/CSF boundary in template space were filtered out (voxels removed if coefficient of variation for either modality, AV-1451 or PIB data, was   .5). A testing mask, representing voxels highly likely to be cortical GM in the PET data, was created from the resulting image. Template space AV-1451 and PiB images were then masked by this testing mask and smoothed by an additional 4 mm FWHM kernel before analysis. We then used BPM (in SPM5) to examine the association between voxelwise PiB and AV-1451, using participant covariates of age, sex, and global GM fraction (bisquare robust regression model; results similar with other robust regression methods). Results were considered significant if passing a one-way false discovery rate (FDR)-corrected threshold of $p < .01$ (k = 10 voxels). BPM result clusters were used as masks to extract mean signal of PiB and AV-1451 voxels within each cluster. A k-means algorithm (k = 2) was used to label each BPM cluster as having either high or low combined PET pathology (based on both mean AV-1451 and PiB); we evaluated the optimal clustering solution in Matlab (2 to 10 clusters inclusive, highest variance ratio criterion; Calinski and Harabasz, 1974). Significant clusters were visualized on a brain template image. These processing and analysis choices focused on testing voxels highly likely to be cortical GM in PET data, and may underestimate local associations, but were designed to minimize the finding of false positive PiB-AV1451 associations. In addition, there may be information loss by considering only mean values from each cluster.

2.7. ROI Analysis Preprocessing and Statistics

In addition to the BPM preprocessing pipeline, we employed an ROI processing pipeline beginning with template-space PET images. Using the MNI-space PET images, and an in-house template-space brain atlas (modified FreeSurfer Desikan-Killiany atlas), we calculated ROI mean signal (on unsmoothed data) in 87 brain regions for PiB and AV-1451, and a global PiB measure (see Table). We first explored the interregional correlations within each tracer; specifically, we examined how PiB or AV-1451 signal in an ROI predicted signal from the same tracer in any other ROI, by creating a correlation matrix using results (r values) from pairwise ROI partial correlations (controlling for age, sex, and global GM fraction [see section 2.4]) investigating both PiB—PiB and AV-1451—AV-1451 relations. We also created a correlation matrix using results (r values) from pairwise ROI partial correlations (controlling for age, sex, and global GM fraction) investigating whether PiB in any ROI was associated with AV-1451 in any (same or other) ROI (i.e., comparing different tracers). Additionally, to better characterize inter-tracer associations for this PiB—AV-1451 analysis, we thresholded all results at $p < .01$ (for ROI results, data were not corrected for

multiple comparisons), and calculated average significant *r* values for each hemisphere in each lobe. Finally, for each brain AV-1451 ROI, we calculated the mean partial correlation Pearson *r* value across all PiB ROIs (e.g., mean *r* value in each column of the correlation matrix), and visualized these mean regional correlation values on a brain image.

3. Results

3.1. BPM Reveals Local Association Patterns between PiB and AV-1451 PET

Multiple cortical brain clusters demonstrated local positive associations where PiB retention predicted AV-1451 retention in the same location, indicating that regional Aβ accumulation is locally positively associated with regional tau accumulation across subjects (Figure 1A). Further, these local positive associations appear to be driven by either high or low underlying levels of Aβ or tau pathology. Examining the mean signal within each BPM result cluster, we found that (Figure 1B) increased AV-1451 uptake was associated with greater PiB uptake in regions with both high and low pathology. We labeled each BPM cluster as having either high or low PET pathology (k-means clustering using both AV-1451 and PiB tracer uptake as input), and visualized these on the brain template (Figure 1C). Regions that showed high overall PET pathology (red clusters) were primarily localized to inferior and lateral temporal lobes, as well as other areas. Regions of low pathology showing significant correlations between the two tracers (blue clusters) were in the temporoparietal junction, the occipital pole, and inferior frontal and parietal lobe.

However, while BPM allows us to examine local regional associations, this method reveals little about the spatial specificity of the described Aβ-tau relations. In particular, based on previous hypotheses, we were interested in investigating how Aβ might potentiate the distant (non-local) "spread" or increased extent of tau. To examine this, we employed the ROI partial correlations approach, with a goal of assessing both local and non-local associations.

3.2. ROI Analysis Reveals Complex Associations between PiB and AV-1451 in Normal Aging

We first explored the interregional correlations within each tracer; specifically, we examined how PiB or AV-1451 signal in an ROI predicted signal from the same tracer in any other ROI, and these results are shown in Figure 2. We observed extensive interregional correlations in the PiB data, such that increases in Aβ in a brain region were strongly associated with increased Aβ across numerous other regions of the brain. The pattern of interregional correlations was more specific and localized for AV-1451 with increases in tau in selective regions (e.g. temporal, frontal, and parietal cortex) being strongly associated with increases in tau among these same regions, particularly for homologous cortical structures. In short, patterns of AV-1451 interregional correlations appeared to be more focal.

The results of partial correlations between PiB and AV-1451 are shown in Figure 3A, for all brain ROIs and a global PiB measure; mean partial correlation *r* values of significant relations across lobe are illustrated in Figure 3B (for age associations with AV-1451 independent of PiB, comparable to Figure 3A, see Inline Supplementary Figure 1, which

demonstrates primarily subcortical and temporal associations between age and AV-1451). Across AV-1451 ROIs, strong positive correlations with PiB uptake across the brain were found for most temporal cortical brain regions (purple ROI labels); in other words, increased PiB uptake in nearly all brain regions was associated with increased AV-1451 uptake in bilateral temporal lobes. There were weaker but still significant associations between PiB and frontal (blue labels) and parietal (cyan labels) AV-1451 uptake. For example, increased PiB uptake in cingulate, frontal, parietal and temporal regions was associated with increased frontal AV-1451, while increased frontal, parietal, and temporal PiB was associated with increased parietal AV-1451. PiB uptake in numerous brain regions was also negatively associated with subcortical (black labels) AV-1451 uptake.

The results shown in the figures above suggest that Aβ-tau relations in normal, healthy aging are complex. To visualize the spatial patterns shown in the correlation matrix, the mean correlation value for each AV-1451 ROI across all PiB ROIs was calculated across participants (the mean r value along each AV-1451 ROI column of the correlation matrix), and projected onto a brain template (Figure 4). Importantly, increased Aβ across multiple brain regions (measured using PiB) was associated with increased tau (measured using AV-1451) in numerous temporal, frontal, parietal, and cingulate lobe regions (hot colors). In particular, there were strong associations between Aβ uptake across the brain and AV-1451 uptake in the bilateral temporal neocortex.

4. Discussion

In this study of cognitively normal older adults, we explored uptake patterns of [11C]PiB and [18F]AV-1451, *in vivo* PET biomarkers for fibrillar Aβ and PHF-tau respectively. We focused on examining statistical relations between regional and voxelwise Aβ and tau accumulation and found that Aβ and tau pathology show significant associations among cognitively normal elderly, with local and non-local positive associations between PiB and cortical AV-1451 prominent among these results. In particular, while BPM revealed local positive associations predominantly in inferior and lateral temporal regions, our ROI correlational analysis (which enabled us to simultaneously examine both local and non-local associations) revealed that increased PiB uptake both within and outside the temporal lobes correlated with increased temporal cortical AV-1451 uptake. These correlations did not seem to be regionally specific with regard to the location of Aβ; that is, regardless of the location of Aβ, Aβ deposition was correlated with tau deposition in the temporal and, to a lesser extent frontal cortex. In addition, correlations among brain regions within tracer were higher for PiB than for AV-1451. These results suggest a regional tau accumulation vulnerability of certain brain regions, particularly the temporal lobes, that is linked to Aβ accumulation in widespread brain regions. Several previous studies using both Aβ and tau PET tracers have not explored the relations between specific regional levels of Aβ accumulation and levels of tau accumulation in the same or different brain structures (Johnson et al., 2015; Ossenkoppele et al., 2016; Schöll et al., 2016; Schwarz et al., 2016), yet these are important to understanding whether and how the accumulation of one protein might influence accumulation of the other, and how disease spread through the brain might occur. Limited data exist which explore these inter-tracer relationships and their impact on normal aging and preclinical AD (e.g., Sepulcre et al., 2016).

The current results can be interpreted in the context of current theories of Aβ and tau pathology in aging and neurodegenerative disease (Small et al., 2008). Both Aβ and tau pathology begin accumulating decades before clinical dementia onset (Price and Morris, 1999; Bateman et al., 2012), and models of the preclinical course of both pathologies indicate long phases of preclinical change with different onsets (Jack et al., 2013). However, the relative importance of Aβ and tau in the brain and their effects on neurodegeneration remain debated and poorly understood.

Previous studies examining relations between Aβ and tau in the brain have predominantly been limited to correlations of pathological findings at autopsy (e.g., Braak and Braak, 1991). This is because *in vivo* examination of the prevalence and extent of both Aβ and tau pathology has not been possible prior to the availability of both Aβ and tau PET ligands. While Aβ PET evidence supports autopsy findings of Aβ deposition, the advent of tau PET has enabled further study of these specific relationships during life. In AD, cross-sectional neuropathological studies suggest that the progression of tau neurofibrillary tangle (NFT) deposition follows a relatively stereotyped temporal and spatial pattern, first affecting transentorhinal cortex, then limbic and other neocortical areas, and then association neocortex (Braak and Braak, 1991; Braak and Braak, 1997; Braak et al., 2006; Serrano-Pozo et al., 2011). Cellular and mouse model studies suggest that tau in its pathological hyperphosphorylated form spreads in a trans-synaptic manner and disrupts functional networks (Liu et al., 2012; Menkes-Caspi et al., 2015). It is also known that some medial temporal lobe (MTL) regions may develop age-related tauopathy in late-life in the absence of Aβ pathology or cognitive impairment (Crary et al., 2014); whether and how this process relates to AD remains controversial (Duyckaerts et al., 2015). Furthermore, the relationship between cognition and Aβ is more tenuous than is the relationship of cognition with tau NFT and with synapse number and size (DeKosky and Scheff, 1990; Nelson et al., 2012).

Tau PET imaging is a new method, and we are aware of only one other report (Sepulcre et al., 2016) investigating *in vivo* local and non-local associations between amyloid and tau in normal elderly, which had several differences in sample, methodology, and results that are important to note. Sepulcre et al. (2016) examined more ($n = 88$) subjects in a similar age range (our sample was approximately 2 years older), with a similar degree of education (average 16 years); our current study, unlike Sepulcre et al. (2016), was designed to include 50% amyloid-positive cognitively normal subjects to ensure variability in subject amyloid deposition. Importantly, while the graph theoretical methods employed in Sepulcre et al. (2016) are fundamentally different from our current BPM and ROI correlational analyses, both approaches are able to assess local (same region) and non-local (different region) associations, and produce converging patterns of results. For example, both methodologies (e.g. Figure 4 of this manuscript, and Figure 6.IV in Sepulcre et al., 2016) demonstrated positive non-local associations between tau, in inferolateral temporal lobe and in lateral frontal and parietal lobe, with amyloid throughout the brain.

We could have observed alternative findings with regards to the identification of local or non-local relationships between Aβ and tau PET. Even though it is known that elevations in tau appear in a focal manner, and Aβ elevations occur in a more global pattern, this does not dictate that Aβ everywhere will correlate with tau where it is located. Without direct

correlational analyses such as this it would be impossible to state whether Aβ-tau relationships were local or distant, or were in fact positively associated.

While the primacy of one pathology over the other is debated, it seems likely that interactions between Aβ and tau lie at the core of the development of brain degeneration and AD (Ittner and Götz, 2011). In the current data, it is clear that Aβ and tau are correlated in multiple brain regions but most strongly in the temporal lobes. This suggests that one influences or induces the other; however, it is not clear which one is primary. Data from autosomal dominant forms of AD strongly suggest an inciting role for Aβ, which appears in the brain as the earliest currently-measured biomarker change (Bateman et al., 2012; Fleisher et al., 2012). In addition, in our results, Aβ across extensive cortical regions is correlated with tau (Figure 3), and Aβ is extensively self-correlated (Figure 2) suggesting that Aβ arises more diffusely and homogeneously but influences tau more locally. This scenario is inconsistent with a process whereby locally distributed tau induces widely distributed Aβ; it seems more likely that the accumulation of Aβ throughout the brain over a long period of time results in local deposition of PHF tau. Nevertheless, we cannot rule out the possibility that in late-onset AD, regional tau accumulation in the medial temporal lobes might affect brain Aβ deposition through some mechanism not detectable through measurement of tau with *in vivo* PET imaging. While considerable evidence supports the idea that Aβ and tau pathology interact to induce synaptic dysfunction and neurodegeneration, much remains to be learned about the precise molecular mechanisms of these interactions (Ittner and Götz, 2011; Spires-Jones and Hyman, 2014), and the current results cannot answer this question.

No matter the direction of the effect, it is likely that there is something about inferolateral temporal lobe that contributes to patterns of selectively increased tau deposition measured using AV-1451. This is likely to reflect an early stage of presymptomatic AD, as it occurs in cognitively normal older people. One possible contributing factor is the temporal lobe's connectivity. It is known that the temporal lobe maintains widespread structural and functional connectivity with other brain regions (Suzuki and Amaral, 1994; Schmahmann and Pandya, 2006; Ranganath and Ritchey, 2012), and temporal lobe tau accumulation may be influenced by Aβ in multiple brain regions through these connections. However, this is unlikely the sole explanation, as the temporal lobe does not appear to be structurally or functionally connected to other brain regions in a fundamentally different way than other regions of association neocortex, from younger to older adults (van den Heuvel and Sporns, 2011; Wang et al., 2012; Power et al., 2013; Brier et al., 2014). Another possibility is that these neurons in inferior and lateral temporal cortex are already developing tauopathy, potentially due to connections with MTL. In other words, MTL—neocortex connectivity could "prime" these regions so that when Aβ is deposited (whether locally or non-locally is not yet known) it promotes tangle formation. It could be that Aβ provides or promotes the mechanism by which tau pathology is coaxed beyond its age-related course into preclinical stages of neurodegenerative disease. Longitudinal imaging data and methods to resolve structural and functional connectivity will be vital to understanding this.

Limitations of the current study include the relatively small sample size, a relatively older cohort, and the cross-sectional nature of the imaging data. Our subjects consistently had a

high level of education, and little is known about *in vivo* amyloid-tau interactions in less well-educated subjects; indeed, the only other comparable study included a sample with a similar level of education (Sepulcre et al., 2016). Also, in our analyses it is possible there is information lost by considering only mean values from each cluster. In addition, while we focused on relations among cortical regions (particularly for AV-1451), future analyses may shed light on the nature and importance of subcortical AV-1451 uptake.

5. Conclusions

In summary, there is regional specificity in PiB—AV-1451 (Aβ-tau) relations in normal aging. Temporal tau is present when Aβ is found in extensive brain regions, while frontal and parietal tau uptake patterns are also less strongly positively associated with regional Aβ. While Aβ may potentiate the spread or extent of tau pathology, the pattern of regional associations is strongly suggestive that vulnerability to this interaction is not the same throughout the brain.

Supplementary Material

Refer to Web version on PubMed Central for supplementary material.

Acknowledgments

Abbreviations

AD	Alzheimer's disease
Aβ	Beta-amyloid
BPM	Biological Parametric Mapping
CT	Computed tomography
DVR	Distribution volume ratio
FDR	False discovery rate
GM	Gray matter
LBNL	Lawrence Berkeley National Laboratory
MMSE	Mini-Mental State Examination
MPRAGE	Magnetization prepared rapid gradient echo
MRI	Magnetic resonance imaging
MTL	Medial temporal lobe

NFT	Neurofibrillary tangle
OA	Older adults
PET	Positron emission tomography
PHF	Paired helical filament
PiB	Pittsburgh Compound B
ROI	Region of interest
ROIs	Regions of interest
SUV	Standardized uptake value
SUVR	SUV ratio

References

Bateman RJ, et al. Clinical and Biomarker Changes in Dominantly Inherited Alzheimer's Disease. N Engl J Med. 2012; 367:795–804. [PubMed: 22784036]

Bennett DA, Schneider JA, Arvanitakis Z, Kelly JF, Aggarwal NT, Shah RC, Wilson RS. Neuropathology of older persons without cognitive impairment from two community-based studies. Neurology. 2006; 66:1837–1844. [PubMed: 16801647]

Braak H, Alafuzoff I, Arzberger T, Kretzschmar H, Del Tredici K. Staging of Alzheimer disease-associated neurofibrillary pathology using paraffin sections and immunocytochemistry. Acta Neuropathol. 2006; 112:389–404. [PubMed: 16906426]

Braak H, Braak E. Neuropathological stageing of Alzheimer-related changes. Acta Neuropathol. 1991; 82:239–259. [PubMed: 1759558]

Braak H, Braak E. Frequency of stages of Alzheimer-related lesions in different age categories. Neurobiol Aging. 1997; 18:351–357. [PubMed: 9330961]

Brier MR, Thomas JB, Fagan AM, Hassenstab J, Holtzman DM, Benzinger TL, Morris JC, Ances BM. Functional connectivity and graph theory in preclinical Alzheimer's disease. Neurobiol Aging. 2014; 35:757–768. [PubMed: 24216223]

Cali ski T, Harabasz J. A dendrite method for cluster analysis. Communications in Statistics. 1974; 3:1–27.

Casanova R, Srikanth R, Baer A, Laurienti PJ, Burdette JH, Hayasaka S, Flowers L, Wood F, Maldjian JA. Biological parametric mapping: A statistical toolbox for multimodality brain image analysis. Neuroimage. 2007; 34:137–143. [PubMed: 17070709]

Chien DT, Bahri S, Szardenings AK, Walsh JC, Mu F, Su M-Y, Shankle WR, Elizarov A, Kolb HC. Early clinical PET imaging results with the novel PHF-tau radioligand [F-18]-T807. J Alz Dis. 2013; 34:457–468.

Crary JF, et al. Primary age-related tauopathy (PART): a common pathology associated with human aging. Acta Neuropathol. 2014; 128:755–766. [PubMed: 25348064]

Dani M, Edison P, Brooks DJ. Imaging biomarkers in tauopathies. Parkinsonism Relat Disord. 2016; 22(Suppl 1):S26–S28. [PubMed: 26299160]

Davis DG, Schmitt FA, Wekstein DR, Markesbery WR. Alzheimer neuropathologic alterations in aged cognitively normal subjects. J Neuropathol Exp Neurol. 1999; 58:376–388. [PubMed: 10218633]

DeKosky ST, Scheff SW. Synapse loss in frontal cortex biopsies in Alzheimer's disease: correlation with cognitive severity. Ann Neurol. 1990; 27:457–464. [PubMed: 2360787]

Delis, DC., Kramer, JH., Kaplan, E., Ober, BA. California Verbal Learning Test–Second Edition, Second Edition. San Antonio: The Psychological Corporation; 2000.

Duyckaerts C, Braak H, Brion J-P, Buée L, Del Tredici K, Goedert M, Halliday G, Neumann M, Spillantini MG, Tolnay M, Uchihara T. PART is part of Alzheimer disease. Acta Neuropathol. 2015

Elman JA, Oh H, Madison CM, Baker SL, Vogel JW, Marks SM, Crowley S, O'Neil JP, Jagust WJ. Neural compensation in older people with brain amyloid-β deposition. Nat Neurosci. 2014; 17:1316–1318. [PubMed: 25217827]

Fleisher AS, et al. Florbetapir PET analysis of amyloid-β deposition in the presenilin 1 E280A autosomal dominant Alzheimer's disease kindred: a cross-sectional study. Lancet Neurol. 2012; 11:1057–1065. [PubMed: 23137949]

Ittner LM, Götz J. Amyloid-β and tau--a toxic pas de deux in Alzheimer's disease. Nat Rev Neurosci. 2011; 12:65–72.

Jack CR, Knopman DS, Jagust WJ, Petersen RC, Weiner MW, Aisen PS, Shaw LM, Vemuri P, Wiste HJ, Weigand SD, Lesnick TG, Pankratz VS, Donohue MC, Trojanowski JQ. Tracking pathophysiological processes in Alzheimer's disease: an updated hypothetical model of dynamic biomarkers. Lancet Neurol. 2013; 12:207–216. [PubMed: 23332364]

Johnson KA, et al. Tau PET imaging in aging and early Alzheimer's disease. Ann Neurol. 2015

Klunk WE, et al. Imaging brain amyloid in Alzheimer's disease with Pittsburgh Compound-B. Ann Neurol. 2004; 55:306–319. [PubMed: 14991808]

Liu L, Drouet V, Wu JW, Witter MP, Small SA, Clelland C, Duff K. Trans-synaptic spread of tau pathology in vivo. PLoS ONE. 2012; 7:e31302. [PubMed: 22312444]

Logan J, Fowler JS, Volkow ND, Wang GJ, Ding YS, Alexoff DL. Distribution volume ratios without blood sampling from graphical analysis of PET data. J Cereb Blood Flow Metab. 1996; 16:834–840. [PubMed: 8784228]

Marquie M, Normandin MD, Vanderburg CR, Costantino I, Bien EA, Rycyna LG, Klunk WE, Mathis CA, Ikonomovic MD, Debnath ML, Vasdev N, Dickerson BC, Gomperts SN, Growdon JH, Johnson KA, Frosch MP, Hyman BT, Gomez-Isla T. Validating novel tau PET tracer [F-18]-AV-1451 (T807) on postmortem brain tissue. Ann Neurol. 2015:1–34.

Mathis CA, Wang Y, Holt DP, Huang G-F, Debnath ML, Klunk WE. Synthesis and evaluation of 11C-labeled 6-substituted 2-arylbenzothiazoles as amyloid imaging agents. J Med Chem. 2003; 46:2740–2754. [PubMed: 12801237]

Menkes-Caspi N, Yamin HG, Kellner V, Spires-Jones TL, Cohen D, Stern EA. Pathological Tau Disrupts Ongoing Network Activity. Neuron. 2015

Mormino EC, Brandel MG, Madison CM, Rabinovici GD, Marks S, Baker SL, Jagust WJ. Not quite PIB-positive, not quite PIB-negative: slight PIB elevations in elderly normal control subjects are biologically relevant. Neuroimage. 2012; 59:1152–1160. [PubMed: 21884802]

Mormino EC, Kluth JT, Madison CM, Rabinovici GD, Baker SL, Miller BL, Koeppe RA, Mathis CA, Weiner MW, Jagust WJ. Alzheimer's Disease Neuroimaging Initiative. Episodic memory loss is related to hippocampal-mediated beta-amyloid deposition in elderly subjects. Brain. 2009; 132:1310–1323. [PubMed: 19042931]

Mormino EC, Smiljic A, Hayenga AO, Onami SH, Greicius MD, Rabinovici GD, Janabi M, Baker SL, Yen IV, Madison CM, Miller BL, Jagust WJ. Relationships between β-amyloid and functional connectivity in different components of the default mode network in aging. Cereb Cortex. 2011; 21:2399–2407. [PubMed: 21383234]

Nelson PT, et al. Correlation of Alzheimer disease neuropathologic changes with cognitive status: a review of the literature. J Neuropathol Exp Neurol. 2012; 71:362–381. [PubMed: 22487856]

Ossenkoppele R, et al. Tau PET patterns mirror clinical and neuroanatomical variability in Alzheimer's disease. Brain. 2016

Power JD, Schlaggar BL, Lessov-Schlaggar CN, Petersen SE. Evidence for Hubs in Human Functional Brain Networks. Neuron. 2013; 79:798–813. [PubMed: 23972601]

Price JC, Klunk WE, Lopresti BJ, Lu X, Hoge JA, Ziolko SK, Holt DP, Meltzer CC, Dekosky ST, Mathis CA. Kinetic modeling of amyloid binding in humans using PET imaging and Pittsburgh Compound-B. J Cereb Blood Flow Metab. 2005; 25:1528–1547. [PubMed: 15944649]

Price JL, Morris JC. Tangles and plaques in nondemented aging and "preclinical" Alzheimer's disease. Ann Neurol. 1999; 45:358–368. [PubMed: 10072051]

Ranganath C, Ritchey M. Two cortical systems for memory-guided behaviour. Nat Rev Neurosci. 2012; 13:713–726. [PubMed: 22992647]

Schmahmann, JD., Pandya, DN. Fiber Pathways of the Brain. New York: Oxford University Press; 2006.

Schöll M, Lockhart SN, Schonhaut DR, O'Neil JP, Janabi M, Ossenkoppele R, Baker SL, Vogel JW, Faria J, Schwimmer HD, Rabinovici GD, Jagust WJ. PET Imaging of Tau Deposition in the Aging Human Brain. Neuron. 2016; 89:971–982. [PubMed: 26938442]

Schwarz AJ, Yu P, Miller BB, Shcherbinin S, Dickson J, Navitsky M, Joshi AD, Devous MD, Mintun MS. Regional profiles of the candidate tau PET ligand 18F-AV-1451 recapitulate key features of Braak histopathological stages. Brain. 2016; 139:1539–1550. [PubMed: 26936940]

Sepulcre J, Sabuncu MR, Becker A, Sperling R, Johnson KA. In vivo characterization of the early states of the amyloid-beta network. Brain. 2013; 136:2239–2252. [PubMed: 23801740]

Sepulcre J, Schultz AP, Sabuncu M, Gomez-Isla T, Chhatwal J, Becker A, Sperling R, Johnson KA. In Vivo Tau, Amyloid, and Gray Matter Profiles in the Aging Brain. Journal of Neuroscience. 2016; 36:7364–7374. [PubMed: 27413148]

Serrano-Pozo A, Frosch MP, Masliah E, Hyman BT. Neuropathological alterations in Alzheimer disease. Cold Spring Harb Perspect Med. 2011; 1:a006189. [PubMed: 22229116]

Small SA, Duff K. Linking Abeta and tau in late-onset Alzheimer's disease: a dual pathway hypothesis. Neuron. 2008; 60:534–542. [PubMed: 19038212]

Spires-Jones TL, Hyman BT. The Intersection of Amyloid Beta and Tau at Synapses in Alzheimer's Disease. Neuron. 2014; 82:756–771. [PubMed: 24853936]

Suzuki WA, Amaral DG. Perirhinal and parahippocampal cortices of the macaque monkey: cortical afferents. J Comp Neurol. 1994; 350:497–533. [PubMed: 7890828]

van den Heuvel MP, Sporns O. Rich-club organization of the human connectome. J Neurosci. 2011; 31:15775–15786. [PubMed: 22049421]

Wang J, Zuo X, Dai Z, Xia M, Zhao Z, Zhao X, Jia J, Han Y, He Y. Disrupted Functional Brain Connectome in Individuals at Risk for Alzheimer's Disease. Biological Psychiatry. 2012

Wechsler, D. Wechsler Memory Scale - Third Edition, Third Edition. San Antonio: The Psychological Corporation; 1997.

Yang X, Beason-Held L, Resnick SM, Landman BA. Biological parametric mapping with robust and non-parametric statistics. Neuroimage. 2011; 57:423–430. [PubMed: 21569856]

Highlights

- Increased Aβ and tau pathology occur even in the brains of cognitively normal people

- We observed regional specificity in Aβ-tau relations using PiB and AV-1451 PET images

- Increased temporal tau is associated with increased Aβ in multiple regions

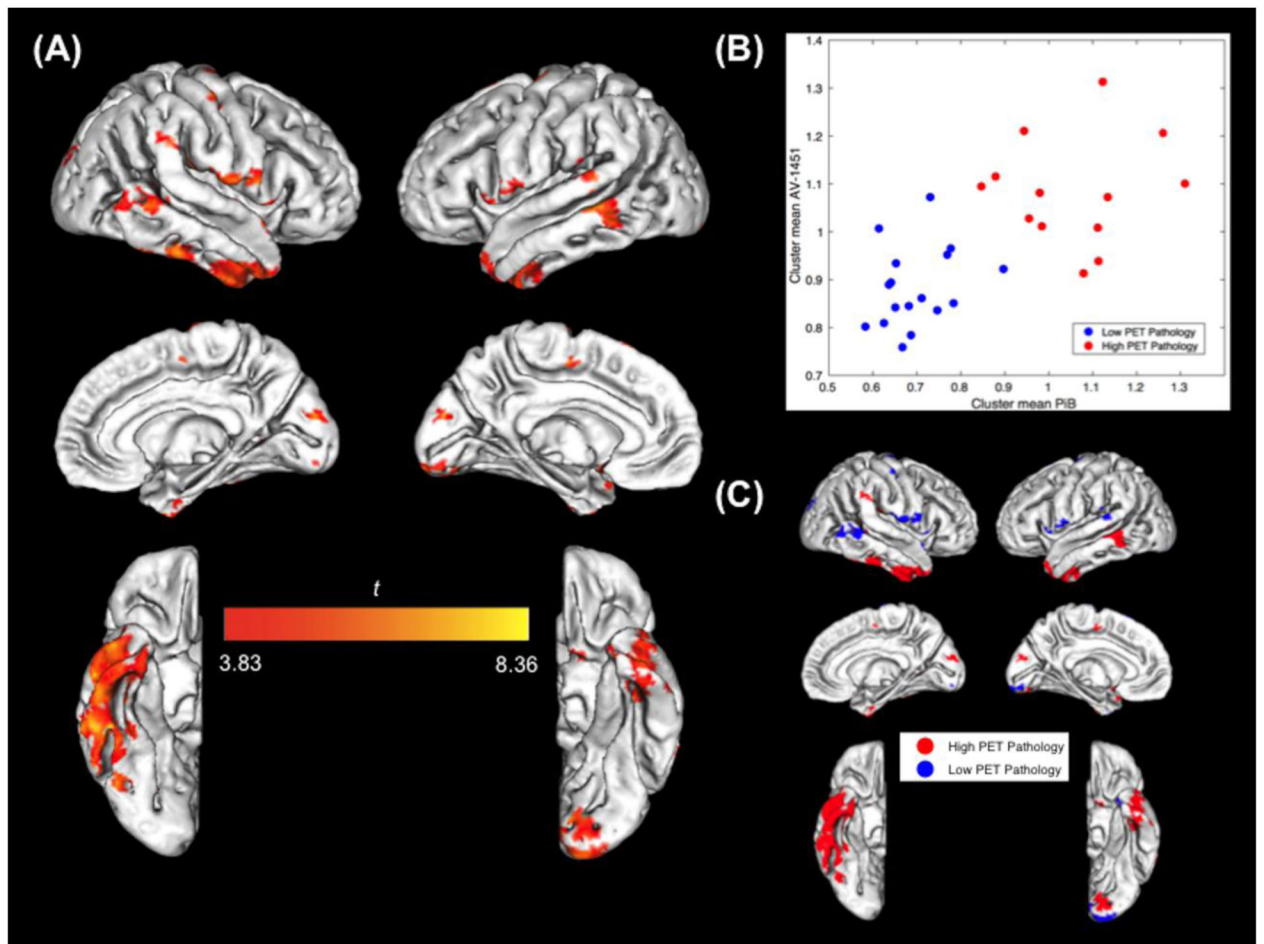- Temporal lobe may be particularly vulnerable to the effects of Aβ

Figure 1. BPM Analysis Results
(A) Significant BPM PiB—AV-1451 associations plotted on template brain image (FDR p < .01; k = 10; covaried for age, sex, and gray matter fraction; data masked (cortical mask) and smoothed (4mm FWHM); bisquare robust regression; right hemisphere on left). (B) Mean signal of PiB and AV-1451 voxels within each BPM result cluster (n = 30). k-means algorithm (k = 2) used to label each BPM cluster as having either high (red) or low (blue) tracer accumulation (based on both mean AV-1451 and PiB). (C) Significant BPM clusters colored as in (B), plotted on template brain image.
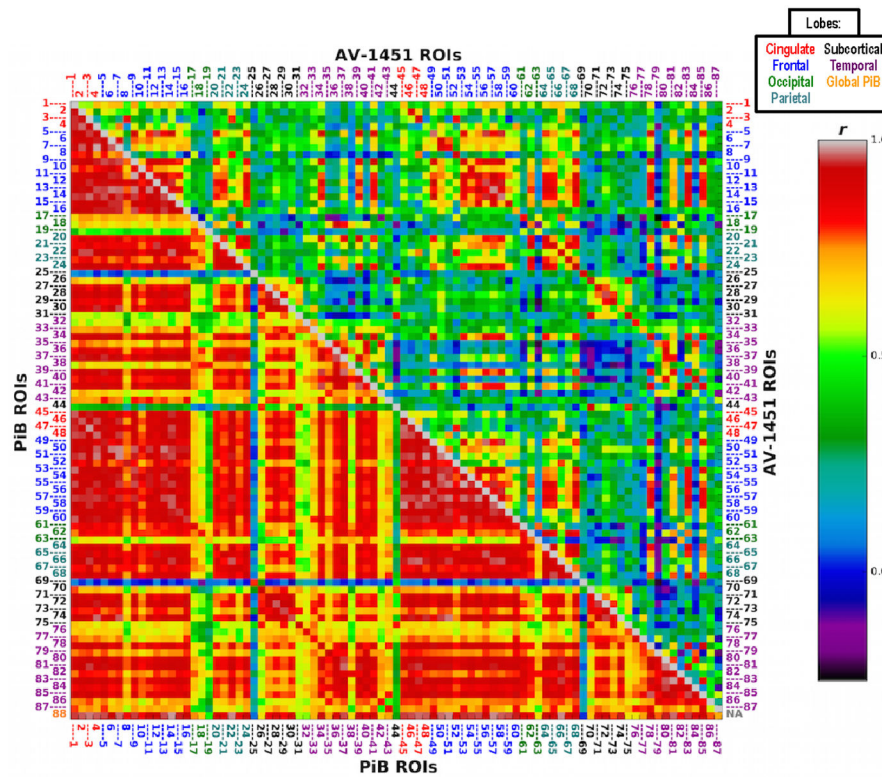
Figure 2. PiB and AV-1451 Intra-tracer ROI Correlation Matrices

Correlation matrix of results (*r* values) from pairwise ROI partial correlations investigating the extent to which each tracer was associated with itself across the brain. Bottom/left: PiB —PiB; top/right: AV-1451—AV-1451. Intra-tracer partial correlation results controlling for ROI values from the opposite modality (for any dependent variable ROI) were largely similar. In-house atlas; MNI 2mm space; covariates of age, sex, global gray matter fraction. ROI descriptions listed in Table. Colors of number labels indicate lobe (see also legend at top of figure): Red: Cingulate lobe; Blue: Frontal lobe; Green: Occipital lobe; Cyan: Parietal lobe; Black: Subcortical; Purple: Temporal lobe; Orange: Global PiB.
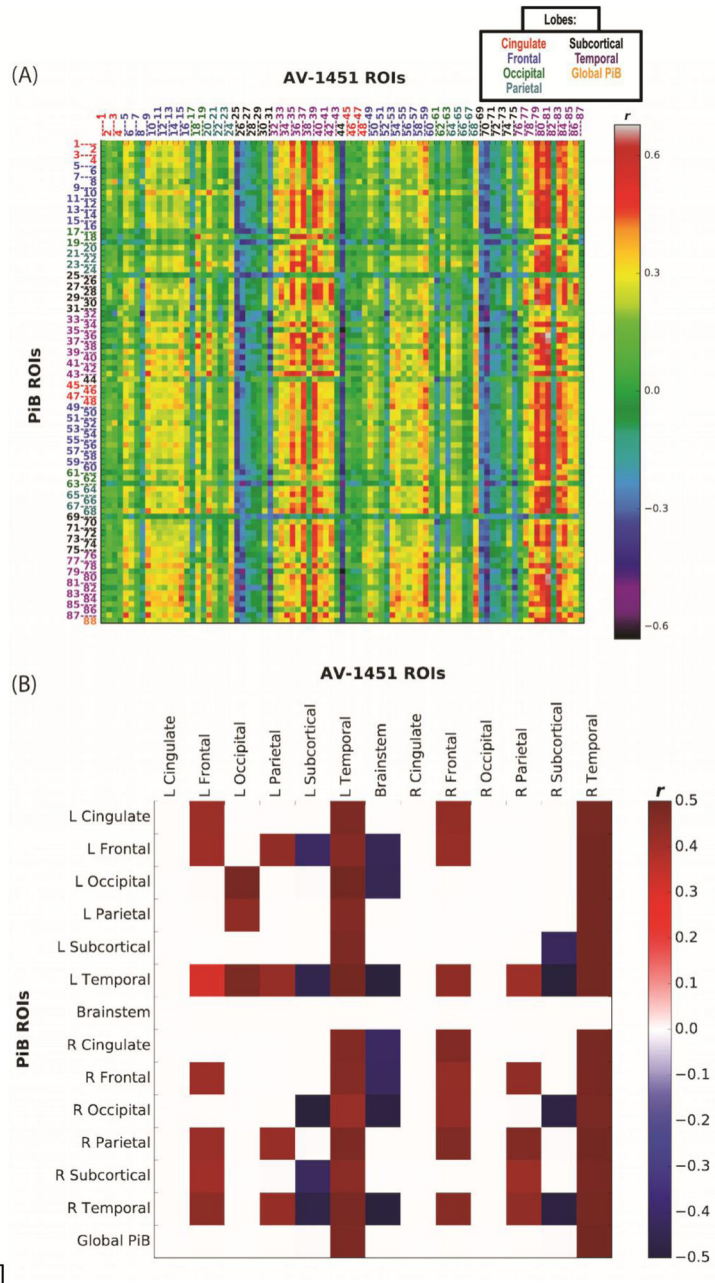
Figure 3. PiB and AV-1451 Inter-tracer ROI Correlation Matrices

(A) Correlation matrix of results (*r* values) from pairwise ROI partial correlations investigating whether PiB in any ROI is associated with AV-1451 in any ROI. In-house atlas; MNI 2mm space; DV = AV-1451; IVs = PiB (ROI values), age, sex, global gray matter fraction. Partial correlation results of PiB and AV-1451 without a global GM volume variable were similar. ROI descriptions listed in Table. Colors of number labels indicate lobe (see also legend at top of figure) and are the same as for Figure 2. (B) Mean partial correlation *r* values of relationships passing *p* < .01 threshold (uncorrected, *n* = 46, averaged across hemisphere and lobe).
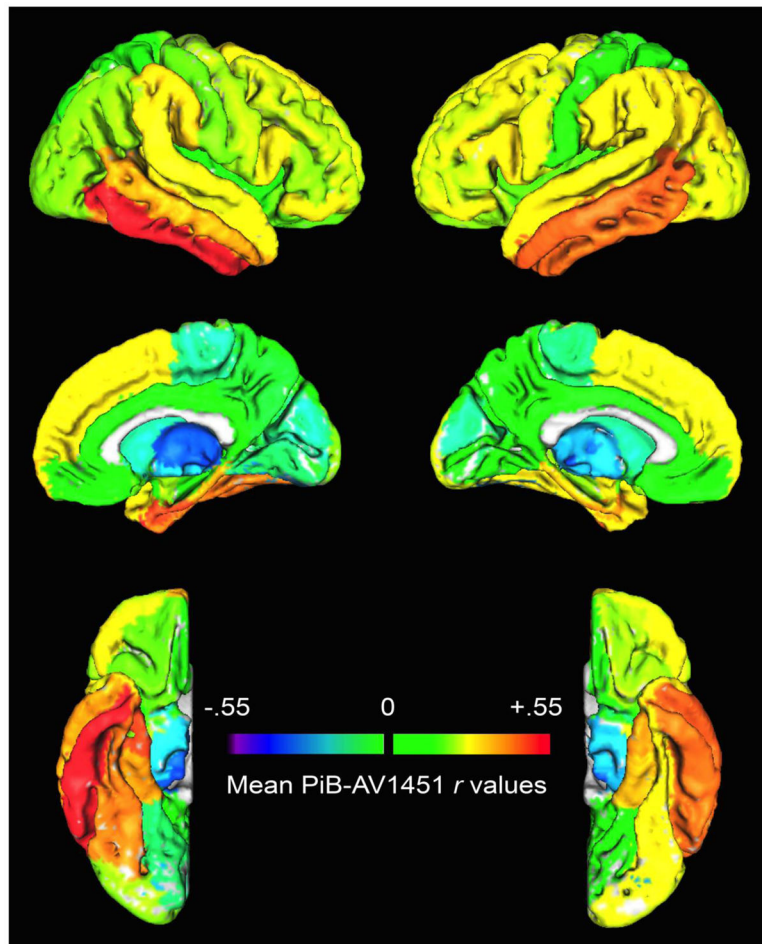
Figure 4. ROI Correlation Analysis Results
Mean partial correlation *r* values (across participants) for each AV-1451 ROI across all PiB
ROIs, plotted on a brain template (right hemisphere on left).

Table

Descriptions of Correlation ROIs.

No.	Lobe	Description	No.	Lobe	Description
1	CL	L caud. ant. CL	45	CL	R caud. ant. CL
2	CL	L isthmus CL	46	CL	R isthmus CL
3	CL	L post. CL	47	CL	R post. CL
4	CL	L rost. ant. CL	48	CL	R rost. ant. CL
5	FL	L caud. middle FL	49	FL	R caud. middle FL
6	FL	L lat. orbital FL	50	FL	R lat. orbital FL
7	FL	L med. orbital FL	51	FL	R med. orbital FL
8	FL	L paracentral	52	FL	R paracentral
9	FL	L pars opercularis	53	FL	R pars opercularis
10	FL	L pars orbitalis	54	FL	R pars orbitalis
11	FL	L pars triangularis	55	FL	R pars triangularis
12	FL	L precentral	56	FL	R precentral
13	FL	L rost. middle FL	57	FL	R rost. middle FL
14	FL	L sup. FL	58	FL	R sup. FL
15	FL	L FL pole	59	FL	R FL pole
16	FL	L insula	60	FL	R insula
17	OL	L cuneus	61	OL	R cuneus
18	OL	L lat. OL	62	OL	R lat. OL
19	OL	L pericalcarine	63	OL	R pericalcarine
20	PL	L inf. PL	64	PL	R inf. PL
21	PL	L postcentral	65	PL	R postcentral
22	PL	L precuneus	66	PL	R precuneus
23	PL	L sup. PL	67	PL	R sup. PL
24	PL	L supramarginal	68	PL	R supramarginal
25	SC	L CB cortex	69	SC	R CB cortex
26	SC	L thalamus	70	SC	R thalamus
27	SC	L caudate	71	SC	R caudate
28	SC	L putamen	72	SC	R putamen

No.	Lobe	Description	No.	Lobe	Description
29	SC	L pallidum	73	SC	R pallidum
30	SC	L accumbens	74	SC	R accumbens
31	SC	L ventral DC	75	SC	R ventral DC
32	TL	L hippocampus	76	TL	R hippocampus
33	TL	L amygdala	77	TL	R amygdala
34	TL	L banks STS	78	TL	R banks STS
35	TL	L entorhinal	79	TL	R entorhinal
36	TL	L fusiform	80	TL	R fusiform
37	TL	L inf. TL	81	TL	R inf. TL
38	TL	L lingual	82	TL	R lingual
39	TL	L middle TL	83	TL	R middle TL
40	TL	L parahippocampal	84	TL	R parahippocampal
41	TL	L sup. TL	85	TL	R sup. TL
42	TL	L TL pole	86	TL	R TL pole
43	TL	L transverse TL	87	TL	R transverse TL
44	SC	B brainstem	88	NA	Global PiB

L = Left; R = Right; B = Bilateral; CL = Cingulate lobe; FL = Frontal Lobe; OL = Occipital Lobe; PL = Parietal Lobe; SC = Subcortical; TL = Temporal Lobe; CB = Cerebellum; Ant. = Anterior; Post. = Posterior; Lat. = Lateral, Med. = Medial; Sup. = Superior; Inf. = Inferior; Caud. = Caudal; Rost. = Rostral; STS = Superior temporal Sulcus.